

Safe Consensus of Cooperative Manipulation with Hierarchical Event-Triggered Control Barrier Functions

Simiao Zhuang, Bingkun Huang, Zewen Yang[†].

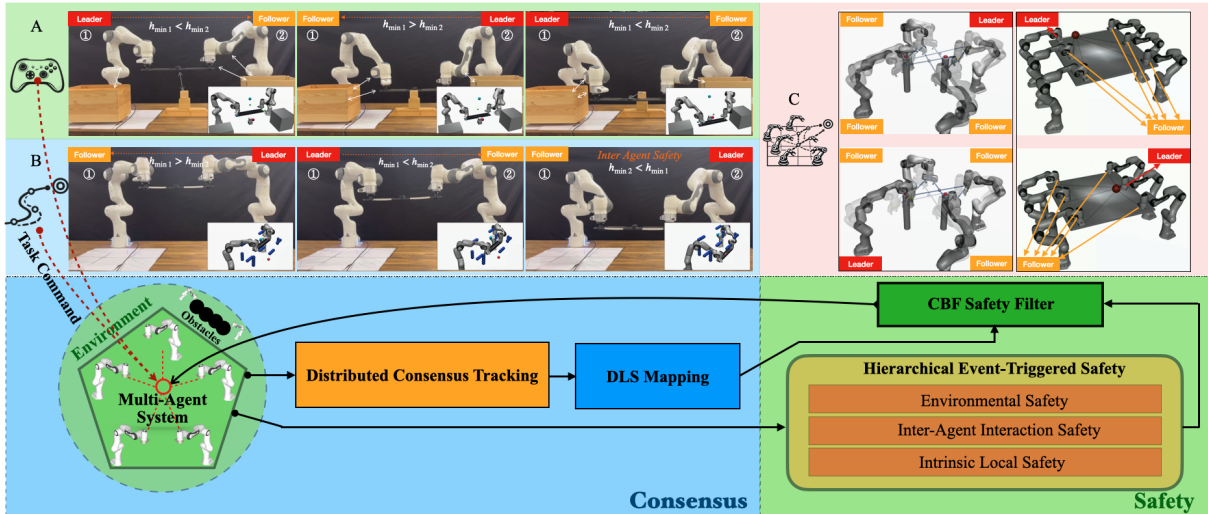


Fig. 1. Overview of the proposed framework. The h_{min} function encodes the minimum distance between the robot and the environmental obstacles.

Abstract—Cooperative transport and manipulation of heavy or bulky payloads by multiple manipulators requires coordinated formation tracking, while simultaneously enforcing strict safety constraints in varying environments with limited communication and real-time computation budgets. This paper presents a distributed control framework that achieves consensus coordination with safety guarantees via hierarchical event-triggered control barrier functions (CBFs). We first develop a consensus-based protocol that relies solely on local neighbor information to enforce both translational and rotational consistency in task space. Building on this coordination layer, we propose a three-level hierarchical event-triggered safety architecture with CBFs, which is integrated with a risk-aware leader selection and smooth switching strategy to reduce online computation. The proposed approach is validated through real-world hardware experiments using two Franka manipulators operating with static obstacles, as well as comprehensive simulations demonstrating scalable multi-arm cooperation with dynamic obstacles. Results demonstrate higher precision cooperation under strict safety constraints, achieving substantially reduced computational cost and communication frequency compared to baseline methods.

I. INTRODUCTION

Multi-agent systems (MASs) enable robots to accomplish tasks that are difficult or infeasible for a single platform,

S. Zhuang, B. Huang, and Z. Yang are with Munich Institute of Robotics and Machine Intelligence (MIRMI), Technical University of Munich (TUM), 80992 Munich, Germany. [†]Corresponding Author <zewen.yang@tum.de >

for instance, when payload weight or size exceeds individual capabilities [1]. In cooperative transport and manipulation, multiple manipulators act as agents physically coupled through a shared payload, yielding a closed-chain system: the team must track a common reference while maintaining prescribed relative end-effector (EE) poses to preserve formation stability [2]. Recent work has developed distributed coordination laws based on consensus and cooperative tracking, enabling team-level objectives using only local neighbor information [3], [4]. However, robust performance remains challenging in practice because safety requirements in cluttered environments, limited communication, and tight real-time computation budgets jointly restrict feasibility and degrade robustness [5]. These challenges motivate cooperative control frameworks that retain the efficiency of distributed coordination while maintaining safety guarantees.

From a coordination viewpoint, cooperative transport and manipulation naturally map to formation objectives, whereas safety necessitates additional constraint enforcement. Each agent must preserve desired relative displacements and poses with respect to its neighbors while the team tracks a reference trajectory [6], [7]. In human-in-the-loop cooperative manipulation, the setting becomes even more demanding: a human partner specifies high-level intent (e.g., a motion direction or target), and the robotic team must autonomously execute the motion while preserving formation consistency

and constrained behavior [8], [9].

A broad range of formation-control methods has been proposed, including virtual-structure methods, leader–follower architectures, and distributed consensus protocols [10]–[12]. Among these, consensus-based control is particularly attractive because it is local and scalable, enabling formation regulation using only neighbor information [13]–[15]. Yet, in safety-critical cooperative manipulation with high-DoF manipulators, tracking and formation maintenance alone are insufficient: the system must also satisfy strict constraints such as obstacle avoidance, inter-agent collision avoidance, and actuator limits under second-order dynamics. This motivates the need for a principled safety mechanism that integrates cleanly with distributed coordination [16], [17].

Control barrier functions (CBFs) have emerged as an effective tool for enforcing safety constraints by rendering a prescribed safe set forward invariant through appropriately designed control laws, often implemented via online safety filtering [18]. For robotic manipulators and MASs with second-order dynamics, input-constrained CBFs provide a systematic way to impose safety requirements in the presence of explicit actuation limits and bounded inputs [19], including scenarios with moving obstacles. By incorporating input bounds directly into the barrier condition, CBFs enforce safety at the actuation level and can reduce conservatism that arises when actuation limits are ignored [20].

Despite these advantages, scaling CBF-based safety filtering to large-scale cooperative manipulation in MASs remains computationally demanding in real time [16], [21]. As the number of agents and collision primitives grows, the number of collision pairs and associated safety constraints increases rapidly, and solving quadratic problems (QPs) at every control step for every agent can become impractical. Especially in time-varying environments, frequent updates of obstacle information further amplify online computation. Therefore, it is necessary to develop a distributed, computationally efficient safety framework that simultaneously enforces formation consistency and collision avoidance for cooperative manipulation.

II. PRELIMINARIES

A. Graph Theory

The communication topology of the MAS is modeled by an undirected graph $\mathcal{G} = (\mathcal{V}, \mathcal{E})$ over $N \in \mathbb{N}$ agents, where $\mathcal{V} = 1, \dots, N$ is the node set indexing the agents and $\mathcal{E} \subseteq \mathcal{V} \times \mathcal{V}$ is the edge set. An edge $(i, j) \in \mathcal{E}$ indicates that agents i and j exchange information bidirectionally. The neighbor set of agent i is defined as $\mathcal{N}_i = \{j \in \mathcal{V} : (i, j) \in \mathcal{E}\}$. The adjacency matrix is $\mathcal{A} = [a_{ij}] \in \mathbb{R}^{N \times N}$, where $a_{ij} = a_{ji} = 1$ if $(i, j) \in \mathcal{E}$, and $a_{ij} = 0$ otherwise. For each agent $i \in \mathcal{V}$, let $\mathbf{p}_i(\cdot) \in \mathbb{R}^3$ and $\mathbf{R}_i(\cdot) \in \text{SO}(3)$ denote the EE position and orientation derived from the forward kinematics map, respectively.

B. System Modeling and Problem Formulation

To address the complexity of cooperative transport, we adopt a hierarchical control architecture that decouples the

high-level consensus planning in the task space from the low-level nonlinear manipulator dynamics in the joint space.

1) Manipulator Dynamics and Task-Space Formulation:

The dynamics of the i -th manipulator follows the standard rigid-body model

$$\mathbf{M}_i(\mathbf{q}_i)\ddot{\mathbf{q}}_i + \mathbf{C}_i(\mathbf{q}_i, \dot{\mathbf{q}}_i)\dot{\mathbf{q}}_i + \mathbf{g}_i(\mathbf{q}_i) = \boldsymbol{\tau}_i, \quad (1)$$

where $\mathbf{q}_i, \dot{\mathbf{q}}_i, \ddot{\mathbf{q}}_i \in \mathbb{R}^n$ denote the joint position, velocity, and acceleration, \mathbf{M}_i , \mathbf{C}_i , and \mathbf{g}_i represent the inertia, Coriolis/centrifugal, and gravity terms, and $\boldsymbol{\tau}_i$ is the control torque.

The coordination objective is defined in task space. Let $\mathbf{x}_i = [\mathbf{p}_i^\top, \boldsymbol{\phi}_i^\top]^\top \in \mathbb{R}^6$ denote the end-effector (EE) pose, where $\mathbf{p}_i \in \mathbb{R}^3$ is the Cartesian position and $\boldsymbol{\phi}_i \in \mathbb{R}^3$ is a minimal orientation representation. The EE twist is $\mathbf{v}_i = [\dot{\mathbf{p}}_i^\top, \boldsymbol{\omega}_i^\top]^\top$.

The differential kinematics is

$$\mathbf{v}_i = \mathbf{J}_i(\mathbf{q}_i)\dot{\mathbf{q}}_i, \quad (2)$$

where $\mathbf{J}_i(\mathbf{q}_i) \in \mathbb{R}^{6 \times n}$ is the geometric Jacobian. Differentiating (2) gives

$$\dot{\mathbf{v}}_i = \dot{\mathbf{J}}_i(\mathbf{q}_i)\dot{\mathbf{q}}_i + \mathbf{J}_i(\mathbf{q}_i, \dot{\mathbf{q}}_i)\dot{\mathbf{q}}_i. \quad (3)$$

2) *Hierarchical Control Design:* We propose a feedback linearization scheme to transform the nonlinear manipulator dynamics into a linear double-integrator system in the task space for formation consensus control. Let $\mathbf{u}_i \in \mathbb{R}^6$ be the virtual control input to be designed by the consensus protocol. The reference joint acceleration $\ddot{\mathbf{q}}_i^{cmd}$ required to track the consensus protocol as

$$\ddot{\mathbf{q}}_i^{cmd} = \mathbf{J}_i^\dagger(\mathbf{q}_i) \left(\mathbf{u}_i - \dot{\mathbf{J}}_i(\mathbf{q}_i, \dot{\mathbf{q}}_i)\dot{\mathbf{q}}_i \right) + \mathbf{N}_i(\mathbf{q}_i)\boldsymbol{\eta}_i, \quad (4)$$

where $\mathbf{J}_i^\dagger = \mathbf{J}_i^\top (\mathbf{J}_i \mathbf{J}_i^\top)^{-1}$ denotes the right Moore-Penrose pseudoinverse, $\mathbf{N}_i = (\mathbf{I}_n - \mathbf{J}_i^\dagger \mathbf{J}_i) \in \mathbb{R}^{n \times n}$ is the null-space projector exploiting the $(n - 6)$ -dimensional redundancy for secondary tasks (e.g., joint limit avoidance, singularity escape), and $\boldsymbol{\eta}_i \in \mathbb{R}^n$ is an auxiliary joint acceleration vector. Substituting $\ddot{\mathbf{q}}_i^{cmd}$ into (1), the control torque is computed via the inverse dynamics law as follows

$$\boldsymbol{\tau}_i = \mathbf{M}_i(\mathbf{q}_i)\ddot{\mathbf{q}}_i^{cmd} + \mathbf{C}_i(\mathbf{q}_i, \dot{\mathbf{q}}_i)\dot{\mathbf{q}}_i + \mathbf{g}_i(\mathbf{q}_i). \quad (5)$$

Substituting (4) into (5) and considering the full-row-rank property $\mathbf{J}_i \mathbf{J}_i^\dagger = \mathbf{I}_6$, it yields the canonical double-integrator dynamics in the task space as follows

$$\dot{\mathbf{x}}_i = \mathbf{v}_i, \quad \dot{\mathbf{v}}_i = \mathbf{u}_i. \quad (6)$$

This formulation reduces the consensus protocol design to specifying \mathbf{u}_i , which is designed in Section III-A. The exact feedback linearization (6) relies on $\mathbf{J}_i \mathbf{J}_i^\dagger = \mathbf{I}_6$. In practice, a numerically robust approximation to \mathbf{J}_i^\dagger is employed near kinematic singularities, as detailed in Section III-B.

3) *Coordination Objective*: In cooperative rigid-body transport, enforcing strict synchronization of both translational and rotational degrees of freedom imposes a fully constrained kinematic coupling among agents. However, manufacturing tolerances, calibration errors, or unmodeled components may introduce inevitable pose discrepancies at the grasp points, where unavoidable pose discrepancies give rise to undesirable internal wrenches that can damage the payload or destabilize the formation. To relax this problem, we propose a practical coordination task that enforces asymptotic positional consensus while relaxing the rotational requirement to a bounded compliance condition. The coordination objective is formalized as follows.

Problem 1 (Practical Consensus Formation):

Consider a linearized double-integrator MASs (6) communicating over a connected undirected graph \mathcal{G} . The object is to design a distributed control law \mathbf{u}_i for each agent $i \in \mathcal{V}$ such that, for all edges $(i, j) \in \mathcal{E}$, the following conditions hold simultaneously:

- *Asymptotic Positional Consensus*: The relative position error converges asymptotically to the prescribed formation offset $\mathbf{d}_{ij} \in \mathbb{R}^3$, i.e.,

$$\lim_{t \rightarrow \infty} \|\mathbf{p}_j(t) - \mathbf{p}_i(t) - \mathbf{d}_{ij}\| = 0. \quad (7)$$

- *Bounded Orientational Consensus*: There exists a finite time $T \in \mathbb{R}_{>0}$ such that the relative angular error $\boldsymbol{\theta}_{ij} \in \mathbb{R}^3$, extracted from the rotation matrix $\mathbf{R}_i^\top \mathbf{R}_j$, satisfies

$$\boldsymbol{\theta}_{ij}(t) \in \Omega_\epsilon := \{\boldsymbol{\xi} \in \mathbb{R}^3 \mid \|\boldsymbol{\xi}\| \leq \epsilon_{\text{ori}}\}, \quad \forall t \geq T, \quad (8)$$

where $\epsilon_{\text{ori}} \in \mathbb{R}_{>0}$ is a small tolerance.

The structure of Problem 1 is both physically motivated and mathematically non-conservative. Regarding condition (7), asymptotic positional consensus is necessary for accurate trajectory tracking of the shared payload. Condition (8) relaxes strict orientational consensus. Because during cooperative transport, each manipulator must resolve obstacle avoidance and joint limit constraints, inevitably resulting in transient rotational deviations that cannot be globally suppressed without sacrificing feasibility. Moreover, the parameter ϵ_{ori} is tunable, where reducing it approaches rigid coordination, while increasing it improves robustness at the cost of rotational accuracy.

4) *Control Barrier Functions*: Consider a nonlinear control-affine system in the form:

$$\dot{\mathbf{s}} = \mathbf{f}(\mathbf{s}) + \mathbf{g}(\mathbf{s})\mathbf{u}, \quad (9)$$

where $\mathbf{s} \in \mathcal{D} \subset \mathbb{R}^n$ is the generic system state and $\mathbf{u} \in \mathcal{U} \subset \mathbb{R}^m$ is the control input. Let $\mathcal{C} \subset \mathcal{D}$ be a safe set defined as the superlevel set of a continuously differentiable function $h : \mathcal{D} \rightarrow \mathbb{R}$, i.e., $\mathcal{C} := \{\mathbf{s} \in \mathcal{D} \mid h(\mathbf{s}) \geq 0\}$ with its boundary $\partial\mathcal{C} := \{\mathbf{s} \in \mathcal{D} \mid h(\mathbf{s}) = 0\}$. The safety of the system is guaranteed if the set \mathcal{C} is *forward invariant*, meaning that for any initial condition $\mathbf{s}(0) \in \mathcal{C}$, the trajectory satisfies $\mathbf{s}(t) \in \mathcal{C}$ for all $t \in \mathbb{R}_{\geq 0}$.

A continuously differentiable function $h : \mathcal{D} \rightarrow \mathbb{R}$ is a CBF for the system (9) if there exists an extended class- \mathcal{K}_∞

function $\alpha : \mathbb{R} \rightarrow \mathbb{R}$ such that, for all $\mathbf{s} \in \mathcal{D}$,

$$\sup_{\mathbf{u} \in \mathcal{U}} [L_f h(\mathbf{s}) + L_g h(\mathbf{s})\mathbf{u}] \geq -\alpha(h(\mathbf{s})), \quad (10)$$

where $L_f h(\mathbf{s}) = \frac{\partial h}{\partial \mathbf{s}} f(\mathbf{s})$ and $L_g h(\mathbf{s}) = \frac{\partial h}{\partial \mathbf{s}} g(\mathbf{s})$ denote the Lie derivatives.

III. METHODOLOGY

A. Distributed Consensus Tracking Protocol

To achieve the two-level coordination objective defined in Problem 1, we design the virtual task-space control input \mathbf{u}_i only based on local neighbor information in \mathcal{N}_i . The control law consists of a control feedback term to maintain geometric formation for high-level planning and a navigational feedforward term to track the group reference for low-level torque control.

For the translational task space, the consensus protocol is designed as a distributed PD-like controller

$$\mathbf{u}_i^{\text{pos}} = - \sum_{j \in \mathcal{N}_i} a_{ij} \left[k_p ((\mathbf{p}_i - \mathbf{p}_j) - \mathbf{d}_{ij}) + k_d (\dot{\mathbf{p}}_i - \dot{\mathbf{p}}_j) \right] - b_i \left[k_p (\mathbf{p}_i - \mathbf{p}_0 - \mathbf{d}_{0,i}) + k_d (\dot{\mathbf{p}}_i - \dot{\mathbf{p}}_0) - \ddot{\mathbf{p}}_0 \right], \quad (11)$$

where $b_i = 1$ if agent i has direct access to the reference state $\mathbf{p}_0, \dot{\mathbf{p}}_0, \ddot{\mathbf{p}}_0$, and $b_i = 0$ otherwise. Moreover, $k_p, k_d \in \mathbb{R}_{>0}$ are the control gains and $\mathbf{d}_{ij} \in \mathbb{R}^3$ is the desired relative displacement from agent i to agent j in task space. Furthermore, the angular acceleration controller is

$$\mathbf{u}_i^{\text{ori}} = - \sum_{j \in \mathcal{N}_i} a_{ij} \left[k_\theta \tilde{\boldsymbol{\theta}}_{ij} + k_\omega (\boldsymbol{\omega}_i - \boldsymbol{\omega}_j) \right] - b_i \left[k_\theta \tilde{\boldsymbol{\theta}}_{0i} + k_\omega (\boldsymbol{\omega}_i - \boldsymbol{\omega}_0) - \dot{\boldsymbol{\omega}}_0 \right], \quad (12)$$

where the world-frame orientation error $\tilde{\boldsymbol{\theta}}_{ij} = \log(\mathbf{R}_i \mathbf{R}_j^\top)^\vee \in \mathbb{R}^3$, $\tilde{\boldsymbol{\theta}}_{0i} = \log(\mathbf{R}_i \mathbf{R}_0^\top)^\vee$ is the orientation error relative to the reference, $\boldsymbol{\omega}_i \in \mathbb{R}^3$ denotes the angular velocity of the EE of agent i , expressed in the world frame, and $k_\theta, k_\omega \in \mathbb{R}_{>0}$ are control gains.

Therefore, the total task-space control input is formed as $\mathbf{u}_i = [(\mathbf{u}_i^{\text{pos}})^\top, (\mathbf{u}_i^{\text{ori}})^\top]^\top \in \mathbb{R}^6$. Note that for agents without direct reference access ($b_i = 0$), the reference trajectory information propagates through the network via the coupling terms. Therefore, to ensure global convergence, the communication graph \mathcal{G} contains a spanning tree [22].

B. Acceleration Mapping via Damped Least Squares

To realize the high-level task-space acceleration command \mathbf{u}_i on the physical manipulator, we must invert the second-order differential kinematics relation (3). Direct inversion of the Jacobian matrix $\mathbf{J}_i(\mathbf{q}_i)$ is prone to numerical instability near kinematic singularities, which can result in excessive joint accelerations and torque demands. To address this, we formulate the inverse kinematics problem as a Tikhonov-regularized optimization that balances task tracking accuracy

against the magnitude of joint acceleration

$$\begin{aligned} \ddot{\mathbf{q}}_i^{\text{task}} = \arg \min_{\ddot{\mathbf{q}} \in \mathbb{R}^n} & \left(\frac{1}{2} \|\mathbf{J}_i(\mathbf{q}_i) \ddot{\mathbf{q}} - (\mathbf{u}_i - \dot{\mathbf{J}}_i(\mathbf{q}_i, \dot{\mathbf{q}}_i) \dot{\mathbf{q}}_i)\|_2^2 \right. \\ & \left. + \frac{\lambda^2}{2} \|\ddot{\mathbf{q}}\|_2^2 \right), \end{aligned} \quad (13)$$

where $\lambda > 0$ is a damping factor. The closed-form solution to this problem provides the robust nominal joint acceleration command

$$\ddot{\mathbf{q}}_i^{\text{task}} = \mathbf{J}_i^\dagger(\mathbf{q}_i) \left(\mathbf{u}_i - \dot{\mathbf{J}}_i(\mathbf{q}_i, \dot{\mathbf{q}}_i) \dot{\mathbf{q}}_i \right), \quad (14)$$

with the damped pseudoinverse defined as

$$\mathbf{J}_i^\dagger := \mathbf{J}_i^\top(\mathbf{q}_i) \left(\mathbf{J}_i(\mathbf{q}_i) \mathbf{J}_i^\top(\mathbf{q}_i) + \lambda^2 \mathbf{I} \right)^{-1}. \quad (15)$$

This formulation ensures that the generated joint acceleration command remains bounded even when the manipulator passes through or near singular configurations. The term $\dot{\mathbf{J}}_i \dot{\mathbf{q}}_i$ compensates for the Coriolis and centrifugal effects in the task space, essential for accurate trajectory tracking in dynamic motions. Finally, the nominal command $\ddot{\mathbf{q}}_i^{\text{nom}} = \ddot{\mathbf{q}}_i^{\text{task}} + \mathbf{N}_i(\mathbf{q}_i) \boldsymbol{\eta}_i$ is passed to the safety filter to enforce strict joint limits and collision constraints, which is detailed in Section III-C.

C. Hierarchical Event-Triggered Safety Architecture

1) *Event-Triggered Environmental Safety*: For manipulators with $n > 6$ degrees of freedom, the forward kinematics map $\mathbf{f}_i : \mathbb{R}^n \rightarrow \mathbb{R}^3 \times \text{SO}(3)$ is not injective. Consequently, the same EE pose $(\mathbf{p}_i, \mathbf{R}_i)$ can be realizable by infinitely many joint configurations, which renders the IK map ill-defined without additional constraints. This non-uniqueness poses a fundamental difficulty for the leader-centric safety framework: the active leader computes the environmental safety constraint on behalf of the entire formation using only task-space states. This consensus fails if agents reside on different branches of the self-motion manifold.

To resolve this, we introduce a null-space regulation law that ensures each agent to a common nominal branch of the self-motion manifold throughout task execution. Specifically, the auxiliary joint acceleration is set as

$$\boldsymbol{\eta}_i = k_{\mathcal{N}} (\mathbf{q}_i^{\text{nom}} - \mathbf{q}_i), \quad k_{\mathcal{N}} \in \mathbb{R}_{>0}, \quad (16)$$

where $\mathbf{q}_i^{\text{nom}} \in \mathbb{R}^n$ is a shared nominal joint configuration satisfying $\mathbf{f}_i(\mathbf{q}_i^{\text{nom}}) = (\mathbf{p}_i^{\text{init}}, \mathbf{R}_0)$. Since $\boldsymbol{\eta}_i$ enters (4) only through the null-space projector \mathbf{N}_i , it has no effect on the task-space dynamics (6) and is therefore fully decoupled from the consensus protocol in Eqs. (11) and (12).

Assumption 1 (Orientation & Null-Space Consensus): The manipulation task commences only after the orientation consensus law (12) and the null-space regulation law (16) have jointly driven all agents to practical synchronization. Formally, there exists a finite time $T_0 \geq 0$ such that for all $t \geq T_0$ and all $i \in \mathcal{V}$:

$$\begin{aligned} \|\tilde{\boldsymbol{\theta}}_{0i}(t)\| &\leq \epsilon_\theta, \quad \|\boldsymbol{\omega}_i(t) - \boldsymbol{\omega}_0(t)\| \leq \epsilon_\omega, \\ \|\mathbf{N}_i(\mathbf{q}_i) (\mathbf{q}_i(t) - \mathbf{q}_i^{\text{nom}})\| &\leq \epsilon_{\text{null}}, \end{aligned} \quad (17)$$

where $\epsilon_\theta, \epsilon_\omega, \epsilon_{\text{null}} \in \mathbb{R}_{>0}$ are prescribed tolerance bounds.

Assumption 1 is practically natural in cooperative manipulation, where all agents are commanded to a common pre-grasp configuration $\mathbf{q}_i^{\text{nom}}$ in multi-arm task planning. The null-space regulation (16) operates purely in the joint space without affecting the EE pose, and can therefore be executed independently by each agent without inter-agent communication. In the limiting case $\epsilon_\theta = \epsilon_\omega = \epsilon_{\text{null}} = 0$, the IK map is locally unique in a neighborhood of $\mathbf{q}_i^{\text{nom}}$ away from kinematic singularities, by the Implicit Function Theorem.

Under Assumption 1, all agents maintain a common nominal branch of the self-motion manifold, ensuring that the sphere centers $\mathbf{c}_{i,k}(\mathbf{q}_i)$ are kinematically consistent across the formation. This allows the active leader to evaluate the environmental safety constraint on behalf of the entire formation. For each agent, the arm geometry is over-approximated by $K_i \in \mathbb{N}$ bounding spheres covering all link bodies, with centers $\mathbf{c}_{i,k}(\mathbf{q}_i) \in \mathbb{R}^3$, $k \in \{1, \dots, K_i\}$, computed via forward kinematics and fixed radii $r_{i,k} \in \mathbb{R}_{>0}$. The signed distance from sphere (i, k) to an obstacle point $\mathbf{o} \in \mathcal{O}$ is

$$\phi_{i,k}(\mathbf{q}_i, \mathbf{o}) := \|\mathbf{c}_{i,k}(\mathbf{q}_i) - \mathbf{o}\| - r_{i,k}, \quad (18)$$

with $\phi_{i,k} \geq 0$ being necessary and sufficient for sphere (i, k) to be obstacle-free.

Assumption 2 (Compact Formation Bound): There exists a constant $\bar{R}_{\text{form}} \in \mathbb{R}_{>0}$ such that for all $t \geq T_0$, all $j \in \mathcal{V}$, and all $k \in \{1, \dots, K_j\}$,

$$\min_{k' \in \{1, \dots, K_\ell\}} \left(\|\mathbf{c}_{j,k}(\mathbf{q}_j) - \mathbf{c}_{\ell,k'}(\mathbf{q}_\ell)\| - r_{\ell,k'} + r_{j,k} \right) \leq \bar{R}_{\text{form}}, \quad (19)$$

where $\mathbf{c}_{\ell,k'}$ are the sphere centers of the active leader $\ell(t)$, and \bar{R}_{form} can be computed offline from the maximum inter-agent separation and the manipulator kinematics.

Assumption 2 states that the entire physical volume of every agent (the union of all bounding spheres) is enclosed within a bounded envelope around the leader body. It is satisfied by design for compact cooperative manipulation formations with bounded inter-agent distances enforced by the consensus protocol (11), and is consistent with Assumption 1 which ensures kinematic predictability of the sphere centers.

Each agent computes its minimum body clearance:

$$d_i^{\text{body}}(t) = \min_{\mathbf{o} \in \mathcal{O}} \min_{k \in \{1, \dots, K_i\}} \phi_{i,k}(\mathbf{q}_i(t), \mathbf{o}) \quad (20)$$

using its own joint state and local obstacle measurements, and broadcasts the scalar d_i^{body} to all agents over \mathcal{G} . The active leader is the agent with the smallest body clearance:

$$\ell(t) = \underset{i \in \mathcal{V}}{\operatorname{argmin}} d_i^{\text{body}}(t), \quad (21)$$

with ties broken by lexicographic order on agent index. Each agent requires only a single scalar broadcast per control step to evaluate (21).

Lemma 1 (Leader-to-Formation Safety Transfer):

Under Assumption 2, for any $\mathbf{o} \in \mathcal{O}$, any $j \in \mathcal{V}$, and any $k \in \{1, \dots, K_j\}$,

$$\phi_{j,k}(\mathbf{q}_j, \mathbf{o}) \geq d_\ell^{\text{body}}(t) - \bar{R}_{\text{form}}. \quad (22)$$

Consequently, $d_\ell^{\text{body}}(t) \geq \bar{R}_{\text{form}}$ implies $\phi_{j,k} \geq 0$ for all (j, k, \mathbf{o}) .

Proof: Let $k^* := \operatorname{argmin}_{k'} \phi_{\ell,k'}(\mathbf{q}_\ell, \mathbf{o})$ be the active leader sphere index. By the triangle inequality, $\|\mathbf{c}_{j,k} - \mathbf{o}\| \geq \|\mathbf{c}_{\ell,k^*} - \mathbf{o}\| - \|\mathbf{c}_{j,k} - \mathbf{c}_{\ell,k^*}\|$. Subtracting $r_{j,k}$ and adding and subtracting r_{ℓ,k^*} , it has

$$\begin{aligned} \phi_{j,k} &\geq \underbrace{\|\mathbf{c}_{\ell,k^*} - \mathbf{o}\| - r_{\ell,k^*}}_{\geq d_\ell^{\text{body}}(t)} - \underbrace{(\|\mathbf{c}_{j,k} - \mathbf{c}_{\ell,k^*}\| - r_{\ell,k^*} + r_{j,k})}_{\leq \bar{R}_{\text{form}} \text{ by (19)}} \\ &\geq d_\ell^{\text{body}}(t) - \bar{R}_{\text{form}}, \end{aligned}$$

which concludes the proof. \blacksquare

By Lemma 1, we design the CBF for the active leader for environmental safety as follows

$$h_\ell^{\text{env}}(\mathbf{q}_\ell) = d_\ell^{\text{body}}(t) - d_{\text{margin}}^{\text{env}} \geq 0, \quad (23)$$

with the safety margin satisfying

$$d_{\text{margin}}^{\text{env}} > \bar{R}_{\text{form}} + \epsilon_{\text{sens}}, \quad (24)$$

where $\epsilon_{\text{sens}} \geq 0$ bounds obstacle sensing uncertainty.

Since d_ℓ^{body} involves a nested minimum over (k, \mathbf{o}) , it is generally non-differentiable. We apply the active-index method, i.e., at each time instant, identify the minimizing pair

$$(k^*, \mathbf{o}^*)(t) := \operatorname{argmin}_{k \in \{1, \dots, K_\ell\}, \mathbf{o} \in \mathcal{O}} \phi_{\ell,k}(\mathbf{q}_\ell, \mathbf{o}), \quad (25)$$

breaking ties by a fixed deterministic rule. At non-smooth instants, Clarke subgradients from $\partial h_\ell^{\text{env}}$ are used, and forward invariance of $\mathcal{S}^{\text{env}} = \{\mathbf{q}_\ell : h_\ell^{\text{env}} \geq 0\}$ is preserved by [23].

Since h_ℓ^{env} depends on \mathbf{q}_ℓ and the closed-loop system exhibits double-integrator task-space dynamics (6), h_ℓ^{env} has relative degree two with respect to \mathbf{u}_ℓ . Define

$$b_\ell^{\text{env}} = \dot{h}_\ell^{\text{env}} + \alpha_1^{\text{env}}(h_\ell^{\text{env}}), \quad \alpha_1^{\text{env}} \in \mathcal{K}_\infty, \quad (26)$$

where $\alpha_1 \in \mathcal{K}_\infty$ is a class \mathcal{K} -infinity and $\dot{h}_\ell^{\text{env}} = (\partial h_\ell^{\text{env}} / \partial \mathbf{q}_\ell) \dot{\mathbf{q}}_\ell$. The second-order CBF constraint

$$\dot{b}_\ell^{\text{env}} + \alpha_2^{\text{env}}(b_\ell^{\text{env}}) \geq 0, \quad \alpha_2^{\text{env}} \in \mathcal{K}_\infty, \quad (27)$$

where $\alpha_2 \in \mathcal{K}_\infty$, is appended to the leader's QP if and only if $\mathcal{E}_\ell^{\text{env}}(t) = 1$. Let $d_{\text{alert}}^{\text{env}} > d_{\text{margin}}^{\text{env}}$ and $\delta_{\text{hyst}}^{\text{env}} > 0$ be the alert distance and hysteresis margin, respectively. Define the scalar trigger function

$$f_\ell^{\text{env}}(t) := d_\ell^{\text{body}}(t) - d_{\text{alert}}^{\text{env}}. \quad (28)$$

The trigger function is designed as

$$\mathcal{E}_\ell^{\text{env}}(t^+) = \begin{cases} 1, & \mathcal{E}_\ell^{\text{env}}(t) = 0 \wedge f_\ell^{\text{env}}(t) \leq 0, \\ 0, & \mathcal{E}_\ell^{\text{env}}(t) = 1 \wedge f_\ell^{\text{env}}(t) \geq \delta_{\text{hyst}}^{\text{env}}, \\ \mathcal{E}_\ell^{\text{env}}(t), & \text{otherwise,} \end{cases}$$

where $\delta_{\text{hyst}}^{\text{env}}$ prevents chattering near the alert boundary. The design parameters satisfy

$$d_{\text{alert}}^{\text{env}} \geq d_{\text{margin}}^{\text{env}} > \bar{R}_{\text{form}} + \epsilon_{\text{sens}}, \quad (29)$$

ensuring the trigger fires *before* h_ℓ^{env} becomes negative, thereby guaranteeing feasibility of (27) upon activation. Leader switches occur when (21) changes value. At each switch instant t_s , the incoming leader ℓ^+ must satisfy

$$h_{\ell^+}^{\text{env}}(\mathbf{q}_{\ell^+}(t_s)) \geq 0, \quad (30)$$

ensuring constraint (27) is initially satisfiable for the new leader. The trigger state $\mathcal{E}_{\ell^+}^{\text{env}}$ is reset to zero and immediately re-evaluated using $\mathbf{q}_{\ell^+}(t_s)$. Stability under switching follows from the dwell-time arguments of [24], provided the minimum dwell time $\tau_{\text{min}} > \tau^*$, where $\tau^* > 0$ is determined by the CBF decay rate α_1^{env} .

2) *Event-Triggered Inter-Agent Interaction Safety:* Inter-agent safety is enforced by ensuring that the EE of every agent i maintains a safe distance from the EEs of all neighboring agents $j \in \mathcal{N}_i$. For each pair (i, j) with $i < j$, define the pairwise EE distance barrier

$$h_{ij}^{\text{inter}} := \|\mathbf{p}_i(\mathbf{q}_i) - \mathbf{p}_j(\mathbf{q}_j)\| - d_{\text{margin}}^{\text{inter}}, \quad (31)$$

where $d_{\text{margin}}^{\text{inter}} > 0$ is the minimum allowable EE separation. Since h_{ij}^{inter} depends on both \mathbf{q}_i and \mathbf{q}_j , it has relative degree two w.r.t. the joint accelerations of both agents. Let $d_{\text{alert}}^{\text{inter}} > 0$ be an alert horizon and $\delta_{\text{hyst}}^{\text{inter}} > 0$ a hysteresis width. Define the pairwise trigger function

$$g_{ij}(t) := \|\mathbf{p}_i(t) - \mathbf{p}_j(t)\| - d_{\text{alert}}^{\text{inter}}, \quad (32)$$

and the symmetric trigger function is

$$\mathcal{E}_{ij}^{\text{inter}}(t^+) = \begin{cases} 1, & \mathcal{E}_{ij}^{\text{inter}}(t) = 0 \wedge g_{ij}(t) \leq 0, \\ 0, & \mathcal{E}_{ij}^{\text{inter}}(t) = 1 \wedge g_{ij}(t) \geq \delta_{\text{hyst}}^{\text{inter}}, \\ \mathcal{E}_{ij}^{\text{inter}}(t), & \text{otherwise,} \end{cases}$$

which is evaluated identically by both agents i and j given that $g_{ij} = g_{ji}$. The design parameters satisfy

$$d_{\text{alert}}^{\text{inter}} \geq d_{\text{margin}}^{\text{inter}} > 0, \quad (33)$$

ensuring the constraint is activated before the barrier becomes negative. When $\mathcal{E}_{ij}^{\text{inter}} = 0$, no state information need be exchanged over edge (i, j) , since the constraint is inactive. Communication is required only when two agents are in close proximity, substantially reducing network load in sparsely occupied workspaces.

3) *Intrinsic Local Safety:* Each agent $i \in \mathcal{V}$ enforces the following intrinsic safety constraints at every control step, independently of the event-triggered mechanism.

- **Joint position limits:** For each joint k , define $h_{i,k}^{q,+} := q_{i,k} - q_{\text{min},i,k}$ and $h_{i,k}^{q,-} := q_{\text{max},i,k} - q_{i,k}$. Both have relative degree two w.r.t. $\ddot{\mathbf{q}}_i$ and are enforced via the HO-CBF condition $\dot{b}_{i,k}^{q,\pm} + \alpha_2(b_{i,k}^{q,\pm}) \geq 0$, where $b_{i,k}^{q,\pm} := \dot{h}_{i,k}^{q,\pm} + \alpha_1(h_{i,k}^{q,\pm})$, $\alpha_1, \alpha_2 \in \mathcal{K}_\infty$.
- **Joint velocity limits:** Define $h_i^v := \dot{q}_{\text{max},i}^2 - \|\dot{\mathbf{q}}_i\|^2$. Since h_i^v has relative degree one, it is enforced by the standard CBF condition $\dot{h}_i^v + \alpha_1(h_i^v) \geq 0$.
- **Torque limits:** The constraint $\tau_{\text{min},i} \leq \tau_i \leq \tau_{\text{max},i}$ is imposed as a box constraint on the QP decision variable via the inverse dynamics law (5).

- Self-collision avoidance: Let $d_i^{\text{self}}(\mathbf{q}_i)$ denote the minimum distance between any non-adjacent link pair of agent i , and let $\delta^{\text{self}} \in \mathbb{R}_{>0}$ be a prescribed safety margin. Define $h_i^{\text{sc}} := d_i^{\text{self}}(\mathbf{q}_i) - \delta^{\text{self}}$, enforced via the same HO-CBF condition as the joint position barriers, using Clarke subgradients at non-smooth instants [23].

For every position-dependent barrier $h_{i,k}(\mathbf{q}_i)$, the HO-CBF condition reduces to the affine constraint in $\ddot{\mathbf{q}}_i$

$$\frac{\partial h_{i,k}}{\partial \mathbf{q}_i} \ddot{\mathbf{q}}_i \geq -\frac{\partial \dot{h}_{i,k}}{\partial \mathbf{q}_i} \dot{\mathbf{q}}_i - \alpha'_1(h_{i,k}) \dot{h}_{i,k} - \alpha_2(b_{i,k}), \quad (34)$$

which is the form directly appended to the unified QP in Section III-C.4.

4) *Unified QP Safety Filter*: At each control step, every agent $i \in \mathcal{V}$ computes a safe joint acceleration by solving the following quadratic program:

$$\ddot{\mathbf{q}}_{\text{safe},i} = \arg \min_{\mathbf{z} \in \mathcal{Z}_i^T} \frac{1}{2} \|\mathbf{z} - \ddot{\mathbf{q}}_i^{\text{nom}}\|^2 \quad (35)$$

s.t. $\dot{b}_{i,k}(\mathbf{q}_i, \dot{\mathbf{q}}_i, \mathbf{z}) + \alpha_2(b_{i,k}) \geq 0, \forall k \in \mathcal{K}_{\text{int},i} \cup \mathcal{K}_{\text{active},i}(t)$,

where \mathcal{Z}_i^T is the torque-feasible set defined the torque limits, $\mathcal{K}_{\text{int},i}$ is the always-active intrinsic constraint index set defined in Section III-C.3, $\mathcal{K}_{\text{active},i}(t)$ is the event-triggered active constraint index set, assembled at each control step from the trigger state machines defined in Section III-C.1 and the inter-agent safety triggers in Section III-C.2. Each constraint in (35) is affine in \mathbf{z} , since

$$\dot{b}_{i,k} = \frac{\partial h_{i,k}}{\partial \mathbf{q}_i} \mathbf{z} + \frac{\partial \dot{h}_{i,k}}{\partial \mathbf{q}_i} \dot{\mathbf{q}}_i, \quad (36)$$

and thus (35) is a strictly convex QP.

Since $d_{\text{alert}}^{\text{env}} \geq d_{\text{margin}}^{\text{env}}$ by (29), each event-triggered CBF constraint is activated only while the corresponding barrier $h_{i,k} > 0$, i.e., strictly inside the safe set. At such instants, $\mathbf{z} = \ddot{\mathbf{q}}_i^{\text{nom}}$ is a feasible point whenever the nominal input satisfies the barrier condition, which holds by construction of the alert threshold. If needed, feasibility can be universally guaranteed by augmenting (35) with a slack variable $\delta_i \geq 0$ and a penalty term $p \delta_i^2$ in the objective.

IV. EXPERIMENTS AND RESULTS

In this section, we evaluate four methods in both real-world experiments and simulations under identical conditions and desired references for quantitative analysis: Ours denotes the proposed HET-CBF framework; Distributed CBF (D-CBF) [25] refers to a baseline where all agents independently solve a CBF-QP safety filter at every control update to enforce both obstacle avoidance and inter-arm collision avoidance; Centralized NMPC [26] is a centralized nonlinear model predictive controller that optimizes the nominal control sequence; Centralized MPPI [27] is a centralized model predictive path integral controller that generates the nominal control sequence.

A. Real World Dual-arm Task

1) *Experimental Description*: The real-world platform consists of two Franka Emika Panda manipulators, each rigidly grasping one end of a transported link to emulate a cooperative transportation scenario. Notably, to ensure collision avoidance of the transported object, each agent treats its end-effector and the proximal half of the link as a unified rigid body, enclosed by a single bounding capsule for safety constraint evaluation. The formation is regulated by a fixed desired relative pose $(\mathbf{d}_{12}^{\text{des}}, \tilde{\boldsymbol{\theta}}_{12}^{\text{des}})$ between the two EEs, where $\mathbf{d}_{12}^{\text{des}} = [0, 0.50, 0]^T$ m and $\tilde{\boldsymbol{\theta}}_{12}^{\text{des}} = [0.32, -0.32, 1.95]^T$ rad. The minimal dwell time $\tau_{\text{min}} = 0.15$ s, and the hysteresis margin is set to $\delta_{\text{hyst}}^{\text{env}}$. The consensus control gains are set as $k_p = 3, k_d = 1, k_\theta = 3, k_\omega = 0.5$. The joint-velocity limit $\dot{q}_{\text{max}} = 2$ rad/s, a damped least-squares factor $\lambda = 0.05$, and the safety margin $d_{\text{safe}} = 0.01$ m. The position and torque limits and self collision configuration are set as the same physical limitation of Franka arms. The task-space reference is defined by the position center of the a transported link $\mathbf{p}_c = 1/2(\mathbf{p}_1 + \mathbf{p}_2)$, whose the target position is set as $\mathbf{p}_g = [0.45, 0.0, 0.3]$. It is generated by a straight-line trajectory in task space obtained by linearly interpolating from the initial $\mathbf{p}_c = [0.24, 0.00, 0.63]^T$ to \mathbf{p}_g and only sent to the active leader defined by $\ell(t)$.

2) *Results*: In Fig. 2, we compare the consensus position error defined as $E_p = 1/N \sum_{i,j \in \mathcal{V}} \|\mathbf{p}_j(t) - \mathbf{p}_i(t) - \mathbf{d}_{ij}\|$ and rotation error denoted by $E_\theta = 1/N \sum_{i,j \in \mathcal{V}} \|\tilde{\boldsymbol{\theta}}_{ij}\|$ across four methods. The shaded intervals indicate which leader is active under the proposed HET-CBF. HET-CBF consistently achieves the smallest E_p over the entire task, staying below 0.005 for most of the execution. In contrast, NMPC settles at a relatively large steady-state error, MPPI shows pronounced oscillations, and the distributed CBF performance deteriorates markedly after 200 steps. For the rotation error E_θ , HET-CBF achieves the lowest values overall. MPPI also keeps the error at a low level, but it exhibits noticeable chattering. Meanwhile, distributed CBF exhibits a peak of about 0.3, and NMPC reduces the error only gradually. Notably, under HET-CBF, E_θ increases around 100 and 700 steps due to obstacle avoidance behavior. This is expected because, in the prioritized objective of the control design (cf. Problem 1), position consensus is enforced as the primary goal, while orientation tracking is treated as secondary.

B. Monte Carlo Experiment

1) *Experimental Description*: To assess robustness, we perform a Monte Carlo trial with $N_{\text{trial}} = 20$ trials of two-arm simulations conducted in MuJoCo in a workspace with the same static sphere-based obstacles in Section IV-A. Moreover, unless otherwise stated, the remaining controller parameters and robotic constraints are the same as in the real-world experiments in Section IV-A. In each trial, we apply small random perturbations to the initial condition, the Cartesian goal position, and the obstacle-sphere centers, and reuse the same randomized trial configuration across all compared methods to enable a paired and fair comparison.

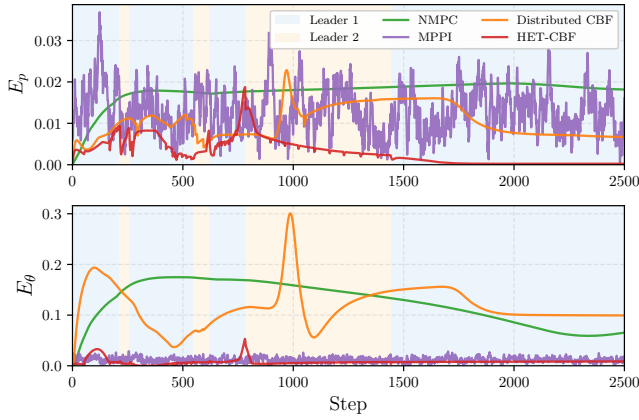


Fig. 2. Comparison of formation position error and orientation error across methods and leader active duration of HET-CBF (shaded regions).

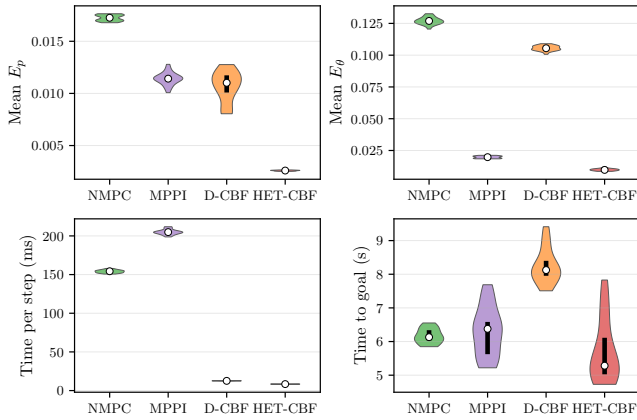


Fig. 3. Monte Carlo evaluation comparing formation position error, orientation error, computational time, and task completion time across methods.

Specifically, the formation-center configuration is perturbed by $\Delta q_c \sim \mathcal{U}[-0.04, 0.04]$ m, the goal position is perturbed per axis by $\Delta p_g \sim \mathcal{U}[-0.02, 0.02]$ m, and each obstacle center is perturbed per axis by $\Delta o_k \sim \mathcal{U}[-0.02, 0.02]$ m.

2) *Results*: In terms of tracking accuracy, HET-CBF achieves the lowest formation position error and orientation error, outperforming NMPC by nearly an order of magnitude and surpassing both MPPI and D-CBF by a substantial margin. Regarding computational efficiency, HET-CBF reduces the per-step solve time to approximately 8 ms over $19\times$ faster than NMPC and $25\times$ faster than MPPI, validating the scalability of the event-triggered QP architecture for real-time deployment. Furthermore, HET-CBF achieves the shortest task completion time with a median of approximately 5.3 s, while D-CBF incurs the highest latency, demonstrating that the hierarchical leader-switching strategy in HET-CBF not only enforces safety but also preserves task efficiency.

C. Multi-arm Task

1) *Experimental Description*: We further evaluate scalability in simulation using a multi-arm cooperative task

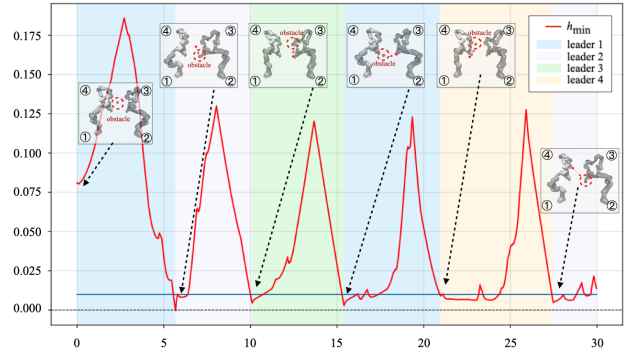


Fig. 4. Visualization of $h_{\min}(t)$ and leader active duration in four-arm scenario.

TABLE I
PERFORMANCE COMPARISON IN FOUR-ARM SIMULATION.

Method	Safety	Time per step (ms)	E_p	E_θ
Ours	✓	3.06 ± 0.51	0.0080 ± 0.0092	0.030 ± 0.072
D-CBF	✓	3.32 ± 0.37	0.011 ± 0.0068	0.039 ± 0.086
NMPC	✗	42.03 ± 7.56	0.036 ± 0.014	0.13 ± 0.090
MPPI	✗	259.2 ± 13.90	0.010 ± 0.0092	0.047 ± 0.062

in MuJoCo. In this scenario, a single dynamic spherical obstacle with an angular velocity of 0.2 rad/s moves along a circular trajectory around the four manipulators, repeatedly approaching the formation and creating time-varying risk. In our method, communication follows a ring topology, where $\mathcal{E} = \{(1, 2), (2, 3), (3, 4), (4, 1)\}$. Unless otherwise stated, the remaining controller parameters are the same as in the real-world experiments in Section IV-A. The team-level task variable is defined as the formation center $\mathbf{p}_c := \frac{1}{4} \sum_{i=1}^4 \mathbf{p}_i = [0.50, 0.00, 0.62]$, and the formation is generated by the initial joint space $[0.0, -0.57, 0.0, -2.14, 0.0, 1.57, 0.79]$ and the base positions are set to $\{[0, \pm 0.50, 0]^\top, [\pm 1.00, \pm 0.50, 0]^\top\}$. The dynamic obstacle follows a circular path with radius $r_{\text{circ}} = 0.30$ m, center and angular speed $\omega_{\text{obs}} = 0.2$ rad/s. We first evaluate the method under human-in-the-loop control, where a user teleoperates the active leader using a world-frame end-effector velocity command of 0.6 m/s, while the remaining agents maintain the formation via distributed consensus. We record the minimum safety barrier value $h_{\min}(t)$, defined as the environmental barrier $h_i^{\text{env}}(t)$ of the arm that is closest to the external spherical obstacle, i.e., $h_{\min}(t) := \min_{i \in \mathcal{V}} h_i^{\text{env}}(t)$ during an execution. Second, we conduct station-keeping experiments in which the multi-arm system maintains its nominal initial pose while avoiding a dynamic spherical obstacle. We quantitatively benchmark the proposed framework against baseline methods in terms of formation accuracy, orientation error, computational cost, and safety compliance (i.e., whether all agents successfully avoid obstacles).

2) *Results*: In Fig. 4, when teleoperating the active leader, the formation motion together with the circularly moving obstacle causes the risk to shift among different arms, leading

to periodic drops in $h_{\min}(t)$. The blue curve indicates the prescribed safety margin d_{safe} . Meanwhile, the active leader rotates among the manipulators and is always assigned to the arm currently closest to the obstacle, ensuring safety throughout the execution, as indicated by $h_{\min}(t) > 0$ at all times. And as shown in Table I, the proposed framework achieves the best performance across all metrics. Only Ours and D-CBF satisfy safety constraints throughout the task, while NMPC and MPPI fail to avoid obstacles. Ours attains the lowest per-step solve time, the smallest position error, and the lowest rotational error, showing that the HET architecture achieves real-time feasibility, strict safety compliance, and superior tracking precision over all baseline methods.

V. CONCLUSION

This paper presented a distributed hierarchical framework for safe cooperative manipulation with multiple manipulators. To enforce strict safety constraints without excessive computational overhead, we developed a three-layer event-triggered architecture that integrates CBFs with a risk-aware leader switching strategy, efficiently distributing safety-critical computation across the network. Real-world experiments with two Franka manipulators validated the framework in real-world static obstacle scenarios, while comprehensive Monte Carlo simulations and four-arm scenarios confirmed its scalability and robustness under dynamic obstacle environments. Compared to state-of-the-art baselines, the proposed framework maintains strict constraint satisfaction and high-precision formation tracking while substantially reducing QP solve times and communication cost.

REFERENCES

- [1] R. Olfati-Saber, J. A. Fax, and R. M. Murray, "Consensus and Cooperation in Networked Multi-Agent Systems," *Proceedings of the IEEE*, vol. 95, no. 1, pp. 215–233, 2007.
- [2] P. B. g. Dohmann and S. Hirche, "Distributed Control for Cooperative Manipulation With Event-Triggered Communication," *IEEE Transactions on Robotics*, vol. 36, no. 4, pp. 1038–1052, 2020.
- [3] Z. Yang, S. Dong, A. Lederer, X. Dai, S. Chen, S. Sosnowski, G. Hattab, and S. Hirche, "Cooperative Learning with Gaussian Processes for Euler-Lagrange Systems Tracking Control Under Switching Topologies," in *2024 American Control Conference (ACC)*, pp. 560–567, 2024.
- [4] X. Dai, Z. Yang, S. Zhang, D.-H. Zhai, Y. Xia, and S. Hirche, "Cooperative Online Learning for Multiagent System Control via Gaussian Processes With Event-Triggered Mechanism," *IEEE Transactions on Neural Networks and Learning Systems*, vol. 36, no. 7, pp. 13304–13318, 2025.
- [5] J. Alonso-Mora, S. Baker, and D. Rus, "Multi-robot formation control and object transport in dynamic environments via constrained optimization," *The International Journal of Robotics Research*, vol. 36, no. 9, pp. 1000–1021, 2017.
- [6] C. R. d. Cos and D. V. Dimarogonas, "Adaptive Cooperative Control for Human-Robot Load Manipulation," *IEEE Robotics and Automation Letters*, vol. 7, no. 2, pp. 5623–5630, 2022.
- [7] H. Farivarnejad and S. Berman, "Multirobot Control Strategies for Collective Transport," *Annual Review of Control, Robotics, and Autonomous Systems*, vol. 5, no. Volume 5, 2022, pp. 205–219, 2022.
- [8] S. Musić, G. Salvietti, P. Budde gen. Dohmann, F. Chinello, D. Prati-chizzo, and S. Hirche, "Robot team teleoperation for cooperative manipulation using wearable haptics," in *Proceedings of the IEEE/RSJ International Conference on Intelligent Robots and Systems (IROS)*, pp. 2556–2563, 2017.
- [9] F. Caccavale, P. Chiacchio, A. Marino, and L. Villani, "Six-dof impedance control of dual-arm cooperative manipulators," *IEEE/ASME Transactions on Mechatronics*, vol. 13, pp. 576–586, Oct. 2008.
- [10] W. Ren, "Consensus strategies for cooperative control of vehicle formations," *IET Control Theory & Applications*, vol. 1, pp. 505–512, 2007.
- [11] Z. Yan, Z. Yang, X. Pan, J. Zhou, and D. Wu, "Virtual leader based path tracking control for Multi-UUV considering sampled-data delays and packet losses," *Ocean Engineering*, vol. 216, p. 108065, 2020.
- [12] Z. Yang, S. Sosnowski, Q. Liu, J. Jiao, A. Lederer, and S. Hirche, "Distributed Learning Consensus Control for Unknown Nonlinear Multi-Agent Systems based on Gaussian Processes," in *2021 60th IEEE Conference on Decision and Control (CDC)*, pp. 4406–4411, 2021.
- [13] Y. Liu and R. Bucknall, "A survey of formation control and motion planning of multiple unmanned vehicles," *Robotica*, vol. 36, no. 7, pp. 1019–1047, 2018.
- [14] D. Roy, A. Chowdhury, M. Maitra, and S. Bhattacharya, "Multi-robot virtual structure switching and formation changing strategy in an unknown occluded environment," in *2018 IEEE/RSJ International Conference on Intelligent Robots and Systems (IROS)*, pp. 4854–4861, 2018.
- [15] G. Lee and D. Chwa, "Decentralized behavior-based formation control of multiple robots considering obstacle avoidance," *Intelligent Service Robotics*, vol. 11, no. 1, pp. 127–138, 2018.
- [16] L. Wang, A. D. Ames, and M. Egerstedt, "Safety barrier certificates for collision-free multirobot systems," *IEEE Transactions on Robotics*, vol. 33, pp. 661–674, June 2017.
- [17] C. Jiang and Y. Guo, "Incorporating control barrier functions in distributed model predictive control for multirobot coordinated control," *IEEE Transactions on Control of Network Systems*, vol. 11, pp. 547–557, Mar. 2024.
- [18] D. Morton and M. Pavone, "Safe, task-consistent manipulation with operational space control barrier functions," *arXiv preprint arXiv:2503.06736*, 2025.
- [19] D. R. Agrawal and D. Panagou, "Safe control synthesis via input constrained control barrier functions," in *2021 60th IEEE Conference on Decision and Control (CDC)*, pp. 6113–6118, 2021.
- [20] Y. Chen, A. Singletary, and A. D. Ames, "Guaranteed obstacle avoidance for multi-robot operations with limited actuation: A control barrier function approach," *IEEE Control Systems Letters*, vol. 5, no. 1, pp. 127–132, 2020.
- [21] W. Luo, W. Sun, and A. Kapoor, "Multi-robot collision avoidance under uncertainty with probabilistic safety barrier certificates," *Advances in Neural Information Processing Systems*, vol. 33, pp. 372–383, 2020.
- [22] R. Olfati-Saber and R. Murray, "Consensus problems in networks of agents with switching topology and time-delays," *IEEE Transactions on Automatic Control*, vol. 49, no. 9, pp. 1520–1533, 2004.
- [23] P. Glotfelter, J. Cortés, and M. Egerstedt, "Nonsmooth Barrier Functions With Applications to Multi-Robot Systems," *IEEE Control Systems Letters*, vol. 1, no. 2, pp. 310–315, 2017.
- [24] D. Liberzon, *Switching in systems and control*, vol. 190. Springer, 2003.
- [25] P. Mestres, C. Nieto-Granda, and J. Cortés, "Distributed Safe Navigation of Multi-Agent Systems Using Control Barrier Function-Based Controllers," *IEEE Robotics and Automation Letters*, vol. 9, no. 7, pp. 6760–6767, 2024.
- [26] S. Hu, E. Babaian, M. Karimi, and E. Steinbach, "NMPC-MP: Real-time Nonlinear Model Predictive Control for Safe Motion Planning in Manipulator Teleoperation," in *2021 IEEE/RSJ International Conference on Intelligent Robots and Systems (IROS)*, pp. 8309–8316, 2021.
- [27] G. Williams, A. Aldrich, and E. Theodorou, "Model Predictive Path Integral Control using Covariance Variable Importance Sampling," 2015.